Simulations of the novel double-Penning trap for MLLTRAP: Trapping, cooling and mass measurements

P. Chauveau, K. Hauschild, A. Lopez-Martens, M. Maccormick, E. Minaya Ramirez, P.G. Thirolf, C. Weber

Simulations of the novel double-Penning trap for MLLTRAP: trapping, cooling and mass measurements

P. Chauveau[a], K. Hauschild[a], A. Lopez-Martens[a], M. MacCormick[b], E. Minaya Ramirez[b], P. G. Thirolf[c], C. Weber[c]

[a]*Centre de Sciences Nucléaires et de Sciences de la Matière (CSNSM), CNRS/IN2P3 et Université Paris Sud 11, UMR 8609, 91405 Orsay Campus, France*
[b]*Institut de Physique Nucléaire d'Orsay CNRS/IN2P3 et Université Paris Sud 11, UMR 8608, 91406 Orsay Campus, France*
[c]*Faculty of Physics, Ludwig-Maximilians University Munich, Am Coulombwall 1, D-85748 Garching, Germany*

Abstract

MLLTRAP is a double Penning trap mass spectrometer that was initially designed to be located at the Maier-Leibnitz-Laboratory (MLL) in Garching (Germany) for high precision mass measurements of exotic nuclei. A second double-trap assembly, dedicated this time to in-trap α decay spectroscopy, has been developed and is the object of this paper. This assembly can optionally replace the current mass-measurement trap electrode assembly during future spectroscopy campaigns at DESIR/SPIRAL2 in France. Though the previous assembly will be the instrument of choice for high-precision mass measurements, the new double-trap has been designed to be compatible with the ToF-ICR and PI-ICR mass measurement techniques in addition to its initial decay spectroscopy purpose, as it would be a significant operational advantage not to have to switch between assemblies on a regular basis. We have undergone a number of simulations to design this double trap system and estimate its future capabilities. These simulations concern the cooling of ions of interest in the first trap, mass measurements in the second trap and the application of the new Decay and Recoil Imaging (DARING) technique to measure lifetimes of first excited nuclear states populated by α decay. The latter will be described in details in a forthcoming publication and thus the present contribution should be considered as "part one" of a two-part article on the design and simulation of the upcoming double-trap system for MLLTRAP. While the cooling and measurement techniques presented in this contribution have been extensively described and simulated in the past, this specific double-trap has a unique geometry, as the central electrode of the second trap has been replaced by a cubic arrangement of four Si-strip detectors. We study here the expected impact of this geometry on the mass measurement capabilities of the future trap.

Keywords: Penning trap, In-trap decay spectroscopy, mass measurement

1. Introduction

Investigating exotic nuclei far-off stability is necessary to validate or constrain many nuclear models operating in different regions of the chart of nuclei. It is a step towards understanding the structure of exotic nuclei and explaining complex astrophysical phenomena. The technological challenges of creating and studying these nuclei are being met in all major radioactive beam facilities in the world through the development of new beams and instruments. Of all the properties of a nucleus, its mass is one of the most fundamental ones, since the mass defect accounts for the sum of all nuclear interactions within. This makes mass measurement an essential (although incomplete) test for any predictive nuclear model.

Electromagnetic traps have been the most successful devices used in mass separation and measurement, owing to long observation times and predictable particle trajectories. A fairly recent and thorough overview of traps and their use in experimental nuclear physics can be found in [1]. In particular, Penning traps have been known to measure

Email address: p.chauveau@gsi.de (P. Chauveau)

the mass of radioactive nuclei with a precision down to $10^{-8} - 10^{-9}$ [2, 3, 4, 5, 6]. Many such setups are already in operation [7, 8, 9, 10, 11, 12, 13] or under construction [14, 15, 16, 17], showing both the need for measuring the ground-state properties of exotic nuclei and the success of the Penning trap in doing so. The review presented in [18] overviews recent ion traps and the masses they have allowed to measure.

As the most recently operational and upcoming facilities explore regions of the chart of nuclei further away from the valley of stability, the increasingly exotic nuclei produced are now always accompanied by large amounts of contaminants, complicating the study of the species of interest. Isobaric contaminants in particular are deleterious to trap-based mass measurements as they are hard to resolve and their own space charge can alter the trajectory of the ion of interest. For this reason most measurement Penning traps used in nuclear physics are preceded by a purification trap to clean the incoming ion bunch. While some systems use an independent magnet for the purification trap [2, 9], most second-generation setups have mounted both traps within the same magnet [8, 11, 13, 14, 17, 19].

MLLTRAP was initially designed for high precision mass measurements of exotic nuclei. The setup uses a 7-T superconducting magnet and was built at the Maier-Leibnitz-Laboratory (MLL) of the Ludwig-Maximilians-University of Munich. It was commissioned off-line using a surface ionisation Rb ion source and proved capable of separating ions with a resolving power of $1.39 * 10^5$ and measuring masses with a statistical precision of $2.9 * 10^{-8}$ [19]. MLLTRAP is currently installed at ALTO in Orsay, France, pending on-line commissioning [20].

Complementary to mass measurements in traps, decay spectroscopy can provide direct insight into the nuclear structure of the daughter nuclei (nuclear level energy, spin, parity) or even the deep electronic structure of an atom. If the setup allows so, measuring the lifetime of some nuclear levels can bring additional information on the nuclear wavefunction. The combination of a Penning trap and particle/γ detectors perfectly befits decay spectroscopy: the Penning trap can be used either to clean the bunch from isobaric or isomeric contaminants and thus provide a purified sample to a post-trap decay station (trap-assisted decay spectroscopy), or to simply confine an ion bunch that then behaves like a point-like source of decay radiation in vacuum (in-trap decay spectroscopy). Of course a double Penning trap can be used for both by performing purification in the first trap and in-trap decay in the second trap.

An alternative double-trap assembly for MLLTRAP is being developed at CSNSM, Orsay, aiming to perform both in-trap decay spectroscopy of heavy α-particle emitters and mass measurements. In order to avoid confusion from here on, we will refer to this assembly as the second/novel tower and to the mass measurement double trap as the first tower. In the novel tower, the usual central ring of the second trap is replaced by a cubic arrangement of four silicon-strip detectors (SSD), and the operational bias of the detectors provides the trapping potential. Because of the strong magnetic field, conversion electrons are very efficiently guided outside the trap, while the comparatively heavy α particles can be detected by the in-trap SSD, allowing unperturbed detection of the α particles. When combined with a position-sensitive detector placed in the fringe field of the 7-T magnet to detect the electrons, this setup allows to implement the new DARING method [21] to measure the lifetime of excited states populated in the α decay of exotic nuclei. This first-of-its-kind double-trap system has already been described by Weber *et al.* in [22, 23, 24], and recent simulations strongly support the feasibility of this lifetime measurement technique [21].

Both assemblies will be commissioned at ALTO using existing or future beams. The neutron rich beams produced by photofission will allow to probe the mass surface near the magic numbers 50 and 82. ALTO currently lacks the necessary beams to test the second tower, although a fusion-evaporation target ion-source system is being studied to synthesise ^{196}Po ($t_{1/2}$ = 5.8s) in the framework of the TuLIP project (Target Ion Source For Short Lived Ion Production, ANR grant 18-CE31-0023). The magnet and its two towers will ultimately be installed at DESIR [25], the low-energy experimental hall of the SPIRAL2 facility [26] at GANIL, Caen, France. There, MLLTRAP will receive beams from the existing SPIRAL facility as well as from the S3 spectrometer [27], which will include very heavy and super-heavy elements as well as neutron-deficient nuclei at or near the N=Z line.

This contribution describes the design of the novel tower and the simulations related to mass measurements with this assembly. Although this tower was not initially intended for mass measurements, we decided to design it with this objective in mind, as having an all-in-one system capable of decay spectroscopy, lifetime measurements and mass

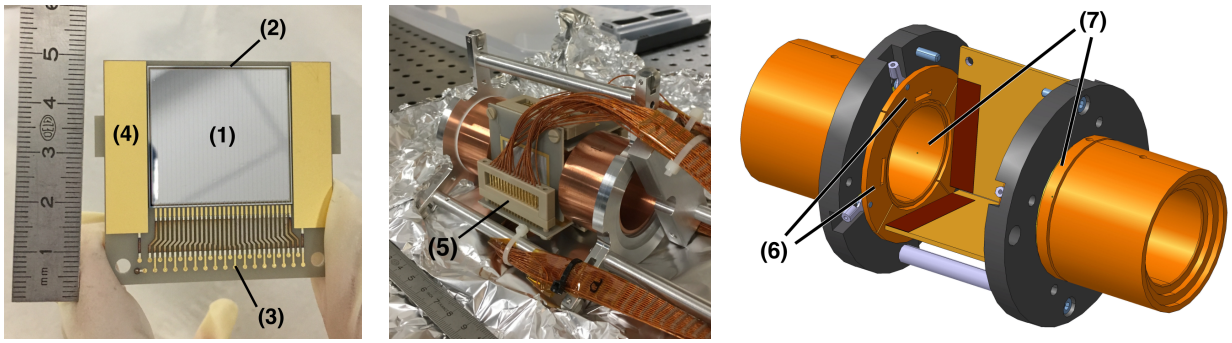

Figure 1: Left, PCB-mounted silicon detector with (1) silicons strips, (2) guard ring, (3) contact pads and (4) gold-plated sections used as correction electrodes. Center, mechanical assembly used at MLL to test the silicon detectors inside the magnet, showing (5) customized PEEK connectors. Right, CAD view of the designed trap structure, featuring (6) segmented support electrodes and (7) side electrodes.

measurements would be an operational advantage. Simulations of the DARING technique completing those already covered in [21] will be detailed in a forthcoming publication. The next section describes the geometry of the double-trap and the features allowing for mass measurements. A brief introduction to Penning trap theory is then given in order to cover the basic equations used in this article. The following section details how the traps were optimised in order to enable mass measurements with the detector-trap. The last section covers the simulation of a typical mass measurement cycle in the second tower with a bunch of 100 ions, from its injection into the first trap to its ejection from the second trap.

2. Geometry of the trap

A precise description of the SSDs has already been given in [23] and a general description of the novel tower is featured in [21]. Here, we give additional details on the design of the second trap. The middle panel of Fig. 1 shows the mechanical assembly of the second trap used at MLL for the tests of the SSD with an α-source. This assembly, however, did not yet allow for trapping. In this configuration the detectors are "plugged" into the copper electrodes using tenon joints. The new geometry is shown in the right panel of Fig. 1 and exhibits several features enabling mass measurements. Although it is clear that the cubic trap breaks the cylindrical symmetry usually found in precision Penning traps, it will be shown that this geometry does not prevent precision mass measurements with the ToF-ICR [28] or PI-ICR [29] techniques.

In order to perform mass measurements or second-stage purification, the spectroscopic trap needs to have segmented electrodes for dipolar and quadrupolar excitation and a high-quality hyperbolic potential. The cubic layout of the trap conveniently provides the four segments required for the excitation. The oscillating potential, usually applied on the central electrode of the trap, will be applied on the flat correction electrodes (**4** on Fig. 1). Since the support electrodes **(6)** in which the tenon joints are inserted are at the same potential as the correction electrodes, they have to be segmented as well. These support electrodes also fulfill the role of a shield, effectively closing the trap box from an electric point of view, in order to cancel any anharmonic contributions that can come from the support rods or cables. Instead of being located next to the side electrodes **(7)**, the support electrodes are wrapped around them, so as to keep the side electrodes close to the trap center. The axial length of these side electrodes has been optimised to reduce the higher order components of the trap's electric field. These changes have been supported by simulations detailed in the next sections. Overall a special attention was given to the shape of the electrodes to avoid direct line of sight between the trapped ions and the insulators so as to prevent them from charging.

3. Penning trap basics

Isobaric cleaning, in-trap decay spectroscopy and precision mass measurements all require to be able to trap ions in a confined space for extended periods of time. Earnshaw's theorem implies that a charged particle cannot be statically

trapped by a purely electrostatic field. It allows, however, a particle to be dynamically trapped in a purely electrostatic field (Multi-Reflection device [30], Orbitrap [31]) in an oscillating electric field (Paul trap [32]) or by a combination of electric and magnetic fields (Penning trap, storage ring). In a uniform, purely magnetic field B, a particle of charge q and mass m revolves perpendicularly to the field axis at the cyclotron frequency:

$$\omega_c = \frac{qB}{m} \tag{1}$$

In a Penning trap, a static harmonic electric field is superimposed on the magnetic field, ensuring axial and radial confinement, respectively. The perfect Penning trap is an especially elegant solution to Earnshaw's theorem: the electric field is static and harmonic in every direction and the stability of an ion inside the trap does not depend on its mass-over-charge ratio or its initial occupation of the phase space. As ω_c (also dubbed the *true cyclotron frequency*) is inversely proportional to the mass, all mass measurement methods in a Penning trap revolve around measuring this frequency. Solving Poisson's equation in vacuum with the harmonicity condition (*i.e.* the potential depends on the spatial dimensions to the second order only) one finds:

$$V(x, y, z) - V(0, 0, 0) = \frac{V_0}{4d^2}(2z^2 - x^2 - y^2) \tag{2}$$

Where d is the characteristic trap dimension calculated from the dimensions of the ring electrode and endcaps [28, 33], and V_0 is the potential difference between these electrodes. When using cylindrical or flat electrodes, the characteristic trap dimension does not match any mechanical length and must be calculated from the shape of the potential itself. The magnetic field is aligned with the z-axis. The motion of a charged particle in such a trap is a combination of three independent eigenmotions of frequencies:

$$\omega_z = \sqrt{\frac{qV_0}{md^2}} \tag{3}$$

$$\omega_+ = \frac{1}{2}\left(\omega_c + \sqrt{\omega_c^2 - 2\omega_z^2}\right) \tag{4}$$

$$\omega_- = \frac{1}{2}\left(\omega_c - \sqrt{\omega_c^2 - 2\omega_z^2}\right) \tag{5}$$

The axial motion of frequency ω_z is simply due to the harmonic electric potential and is of the order 50 kHz for very heavy ions, depending on the trapping potential. The two radial motions of frequency ω_+ and ω_- are called reduced cyclotron motion and magnetron motion, respectively. The superposition of the electric field onto the magnetic field slightly modifies the pure cyclotron motion and thus its frequency, hence the name. However, ω_+ remains very close to ω_c and is therefore almost perfectly linearly dependent on the mass ($\simeq$ 400 kHz at 250 amu). The slow magnetron motions originates from the $\mathbf{E} \times \mathbf{B}$ drift in an axially symmetric field and its frequency can be approximated to first order by $\omega_- \simeq V_0/2Bd^2$ (i.e. $1 - 5$ kHz depending on the potential) and is therefore almost independent of the mass. Equations (4) and (5) yield

$$\omega_+ + \omega_- = \omega_c \tag{6}$$

and

$$\omega_+^2 + \omega_-^2 + \omega_z^2 = \omega_c^2 \tag{7}$$

Eq. (6) implies that an excitation at the true cyclotron frequency can couple the two radial motions. This equality is, however, affected by imperfections in the electric field. Eq. (7) is generally used in the highest precision applications, as it is little sensitive to small trap imperfections [33]. Indeed, in a real trap, the potential differs from the one given in Eq. (2). The true potential around the trap center can be conveniently expressed in spherical coordinates as:

$$V(r, \theta, \phi) = \frac{V_0}{2} \sum_{l,k} C_{l,k} \left(\frac{r}{d}\right)^l P_l^k(cos\theta) cos(k\phi) \tag{8}$$

with P_l^k being the associated Legendre polynomial of degree l and order k with $-l < k < l$ [1]. From here on, we arbitrarily fix $d = 10$ mm and calculate an equivalent V_0 so that $C_{2,0} = 1$. This allows to have comparable $C_{l,k}$ for traps with different geometries or voltage settings. In a perfect trap, the only non-zero coefficients are $C_{0,0}$ and $C_{2,0}$ and effectively, optimising a trap is equivalent to minimising or canceling all coefficients but these two. Imperfections of the electric and magnetic fields affect the eigenmotions and their frequency, thus possibly impairing the mass measurement capabilities of a trap. The precise effect of these imperfections on the different eigenfrequencies has already been described through a quantum mechanical approach [33, 34] and a classical one [35].

One can notice that several of these coefficients are already cancelled owing to symmetries in the trap. Symmetry along the z-axis cancels the terms of odd l, while cylindrical symmetry guarantees that $C_{l,k} = 0$ for all $k \neq 0$. Thus in most cases, the study of trap imperfections is limited to $C_{4,0}$ and $C_{6,0}$, higher order terms being neglected [29, 33, 34, 36, 37, 38]. Since in our case neither of the two traps from the novel tower are perfectly symmetric along the z-axis, the odd l coefficients will be discussed as well. In the second trap the cubic arrangement of the SSDs forces us to consider the $k \neq 0$ coefficients, but the azimuthal $\pi/2$-periodicity imposes that k must be an integer multiple of 4.

Following the method shown in [33, 34], one can calculate the shift in energy due to the terms of even l and deduce the resulting shifts in eigenfrequencies. In the second trap, it can be proven that the energy shift, and thus the frequency shift, due to the first $k \neq 0$ terms $C_{4,4}$ and $C_{6,4}$ is zero. Therefore, we only need to consider the $C_{l,0}$ coefficients, or simply C_l. The impact of the term C_4 on the sum frequency is:

$$\Delta(\omega_+ + \omega_-)_{C_4} = \frac{3C_4\omega_z^2}{4d^2(\omega_+ - \omega_-)}[\rho_-^2 - \rho_+^2] \tag{9}$$

And the one of C_6:

$$\Delta(\omega_+ + \omega_-)_{C_6} = \frac{30C_6\omega_z^2}{16d^4(\omega_+ - \omega_-)}[3z^2(\rho_-^2 - \rho_+^2) + (\rho_+^4 - \rho_-^4)] \tag{10}$$

Where ρ_+ and ρ_- are the radii of the reduced cyclotron and magnetron motions, respectively. These equations show that the sum frequency will be equal to the true cyclotron frequency only when $\rho_+ = \rho_-$. This happens only punctually during the conversion of a radial motion into another, but is generally not the case for any mass measurement procedure inside a Penning trap. Therefore all C_l coefficients should be minimised to reduce the frequency shift between the measured sum frequency and the actual true cyclotron frequency, and thus allow for unbiased mass measurements. In the next section we describe how the potentials of both traps of the second tower were optimised.

4. Trap optimisation

We optimised the potentials of the different electrodes of both traps in order to enhance the quality of the electrostatic field. Practically, the first trap will be used for cooling and isobaric purification but not for mass measurement, which diminishes the interest of a precise potential optimisation. Indeed the mass resolution of the sideband cooling technique is typically a factor 50 larger than for ToF-ICR spectrometry for identical trapping times [28]. However, optimising the first trap is interesting for two main reasons:

- The mass measurement tower is composed of two identical cylindrical traps. Thus an optimisation of the first trap of the spectroscopy tower is valid for the second trap of the mass measurement tower and the calculated potentials could be used as a starting point for a manual optimisation.
- Simulated measurements of the cyclotron frequency in the first trap improve in accuracy after optimisation of the potentials (see further) and the frequency shift is consistent with the experimental mass precision measured during the offline tests [19]. This serves as a proof-of-principle for the optimisation and supports the performance expectation of the second trap.

[1] The order of the associated Legendre polynomials is almost always referred to as "m" in the literature. We chose to use "k" here instead to avoid confusion with the mass.

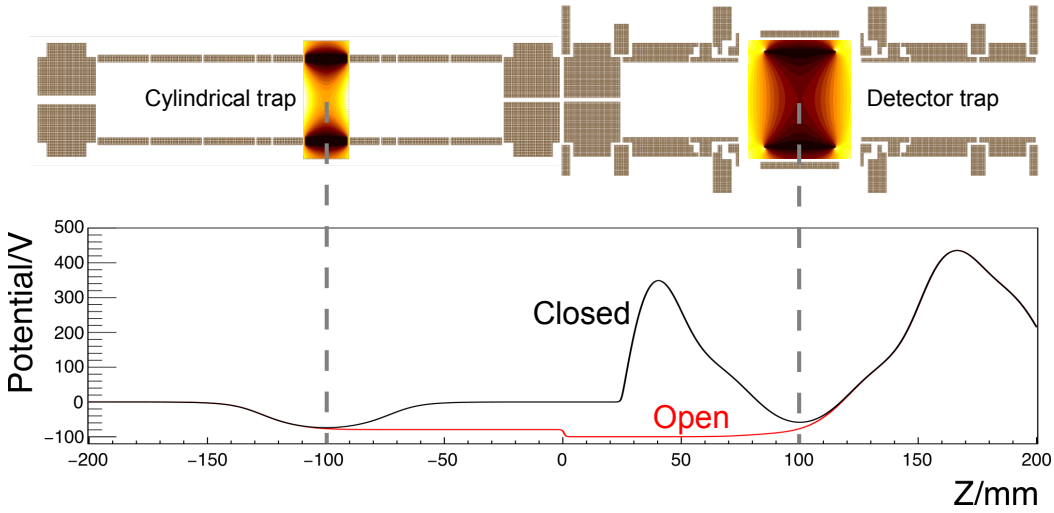

Figure 2: Top, SIMION view of the two-trap system. The potential maps of each trap have been superimposed and exhibit the expected hyperbolic equipotentials. Bottom, potential along the beam axis. The potential depth of the second trap results from the optimisation after imposing a 100 V difference between the silicon strips and the guard rings.

In the second trap, the axial lengths of the first two side electrodes were also optimised. From Eq. (2), we see that the quantity

$$H = \frac{V(x,y,z) - V(0,0,0)}{(x^2 + y^2 - 2z^2)} \tag{11}$$

must be a constant in an ideal Penning trap. We thus chose to optimise the different potentials by minimising the goal function $\sigma_H / < H >$ over a certain volume near the trap center. This simple minimisation parameter allows quick and robust optimisation, though it does not give any direct insight on the mass measurement capabilities of a trap. Indeed $\sigma_H / < H >$ is a global parameter calculated over a volume and depends on the different $C_{l,k}$ coefficients. Yet, as seen before, each of these components has a different influence on the sum frequency $\omega_+ + \omega_-$, therefore the frequency shift is correlated to $\sigma_H / < H >$ but cannot be derived from it. We thus decided to optimise the field with this parameter and check *a posteriori* the effect of this optimisation on the cyclotron frequency by simulation. Practically, $H(x,y,z)$ was calculated at regularly spaced points in the trap using the potential array V built by the Poisson solver of SIMION 8.1 [39], and the goal function was minimised using the ROOT-implemented version of the MINUIT algorithm [40]. The potentials along the z-axis are shown in Fig. 2.

The coefficients C_1 to C_6 have been calculated from the potential array for both traps after optimisation and are reported in Table 1. We also included the results obtained with the potential set used in [19] for comparison (Non optimised or NO in the table). For the first trap, one can see that the optimisation decreased the even order coefficient and increased the odd ones. However, since odd components are very small by construction compared to even components, their impact is comparatively small. Also the first order parameter C_1 only slightly shifts (of the order of nanometers) the position of the potential center but does not impact the frequencies. In addition, it was shown in [33] that the combination of first and third orders yields a frequency shift in the eigenfrequency ω_z, which affects ω_- and ω_+ but not the sum frequency. In the detector trap, the even order coefficients are comparable to those of the optimised first trap. The great difference in odd order terms between the two traps is due to the absence of a collimator on the exit side of the second trap, thus breaking the axial symmetry, while the first trap has collimators on both sides.

Figure 3 shows the simulated and theoretical shift in the frequencies of the radial motions. Simulations of the ion trajectories were done with SIMION and the fact that they mostly follow the theoretical trends demonstrates their reliability. The effect of the optimisation in the first trap is striking, as it almost cancels the frequency shifts. However, one can notice that the frequency shift in the second trap is much larger than in the first trap when both are optimised,

	First Trap		Second Trap
	NO	O	O
σ_H/H	$9.84\ 10^{-3}$	$1.56\ 10^{-3}$	$4.17\ 10^{-3}$
C_1	$1.09\ 10^{-7}$	$3.02\ 10^{-7}$	$7.77\ 10^{-6}$
C_2	1.0	1.0	1.0
C_3	$4.10\ 10^{-8}$	$1.14\ 10^{-7}$	$1.23\ 10^{-4}$
C_4	$-1.01\ 10^{-2}$	$1.07\ 10^{-3}$	$8.82\ 10^{-4}$
C_5	$4.75\ 10^{-9}$	$1.31\ 10^{-8}$	$1.33\ 10^{-5}$
C_6	$-6.78\ 10^{-3}$	$-5.61\ 10^{-3}$	$-9.38\ 10^{-3}$

Table 1: Comparison of the C_l coefficients and the optimisation goal function σ_H/H for non-optimised (NO) and optimised (O) sets of potentials for both traps.

while having comparable C_l and even a smaller C_4. This is due to the fact that the shifts are proportional not only to the C_l coefficients, but also to the depth of the potential well, which is typically 5.4 times bigger in the second trap. Although we chose to show the frequency shifts with the same axial amplitude in both traps, it should be noticed that it should be smaller in the second trap for the same trapping energy. Should the axial amplitude in the second trap be reduced, the corresponding frequency shifts would be reduced as well, though not uniformly for all $\rho_{+/-}$.

With the Phase Imaging Ion Cyclotron Resonance technique (PI-ICR) [41], ions are excited to a quasi pure radial motion (either magnetron or reduced cyclotron) and then accumulate the phase from which the frequency of the corresponding motion can be deduced. If indeed ρ_- can be neglected while measuring ω_+ and ρ_+ can be neglected while measuring ω_-, then the theoretical frequency shifts are symmetric (as can be seen in Equations (9) and (10) and Figure 3) and the net effect on the sum frequency is 0. However, it was still important to minimise C_4 and C_6 as the ρ-dependency of the frequency could induce a smearing of the ion bunch after the phase accumulation and thus limit the precision of the mass measurement [29].

It can be noticed in Figure 3 that the cyclotron frequency shift in the second trap follows nicely its theoretical lineshape, while the magnetron frequency shift steers away from it. In order to investigate this unexpected asymmetry we repeated the same simulations in SIMION, ignoring this time the potential calculated from the geometry and using instead a theoretical potential of our choice. This way, it was possible to artificially "turn on and off" the coefficients C_4, C_6, $C_{4,4}$ and $C_{6,4}$ to identify which was responsible for this effect. The additional frequency shift on the magnetron motion was observed to depend only on $C_{4,4}$ and to be proportional to $C_{4,4}^2$, which is quite remarkable since until now all calculated frequency shifts depended linearly on the C_l. Thus this result does not contradict the previous statement that the expected frequency shifts due to non-cylindrical components should be 0, as this calculation was only considering linear dependencies on the C_l coefficients [2].

By summing the reduced cyclotron and magnetron frequency shifts, we can estimate that the systematic error in the estimation of the true cyclotron frequency is $5.3 * 10^{-8}$ at a radius of 1 mm and $32 * 10^{-8}$ at 2 mm. For comparison the systematic error in the first trap is $3.2 * 10^{-8}$ at both radii, in both optimised and non-optimised configurations. Nevertheless, for small motion radii typically used in PI-ICR (< 1 mm), our cubic geometry is still comparable to a cylindrical Penning trap regarding the frequency shifts, the ρ-dependency of those shifts and the systematic error on the sum frequency.

The Time of Flight Ion Cyclotron Resonance technique (ToF-ICR) [28] raises different issues, as it does not feature a pure radial motion during most of the procedure. During a typical cycle of a ToF-ICR measurement, an initially pure magnetron motion is converted to a pure reduced cyclotron motion by a quadrupolar RF excitation. The motion conversion becomes resonant when the excitation frequency ν_{rf} is close to the sum frequency. Because the

[2] In [35] for example, these have been called "first order frequency shifts", but we avoid this term here to avoid confusion with the order k of the Legendre polynomial.

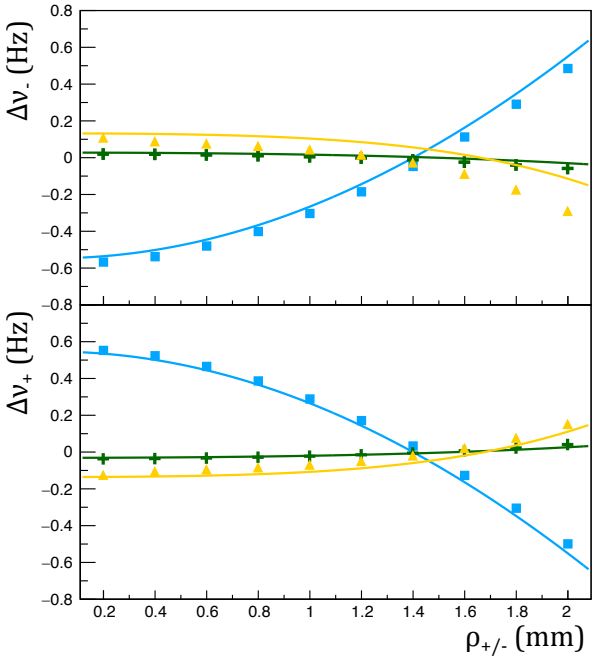

Figure 3: Simulated deviations of the magnetron (top) and reduced cyclotron (bottom) frequencies from the expected values in an ideal Penning trap as a function of the corresponding motion radius. Frequency deviations are shown for the non-optimised first trap (blue squares), optimised first trap (green crosses) and optimised second trap (yellow triangles). The magnetron (resp. reduced cyclotron) frequency has been obtained by simulating a trajectory with mixed magnetron (resp. cyclotron) and axial motions and measuring the accumulated phase of the radial motion over a 200 ms period. The amplitude of the axial motion was 1 mm in all cases. The curves of matching colour and trend are the theoretical frequency shifts calculated from Equations (9) and (10) and the C_4 and C_6 coefficients from Table 1.

energy of the magnetron motion is negligible in comparison to the one of the reduced cyclotron motion in such electric and magnetic fields, the conversion resonance leads to an energy resonance that can eventually be measured by ToF. Without initial cyclotron motion, the two motion radii are related through:

$$\rho_-^2(t) = \rho_-^2(0) - \rho_+^2(t) \tag{12}$$

Provided that the excitation potential is constant, the radii of both these motions follow two beating curves of opposite phase [28] and match each other only once per conversion cycle. This means that the frequency shifts expressed in Equations (9) and (10) cancel for a very short time and that the excitation is off-resonance during most of the motion conversion. However, for a complete conversion, $\Delta(\omega_+ + \omega_-)_{C_4/C_6}$ will be time-antisymmetric with respect to the point $\rho_+ = \rho_-$ and thus the average deviation at the resonance frequency due to (9) and (10) will be 0.

We simulated with SIMION the motion conversion of a single ion with an initially pure magnetron motion in both traps. Figure 4 (top) shows the well known energy vs frequency resonance for the optimised first trap and fitted by the theoretical curve from [28]. If the excitation frequency is different from the unperturbed cyclotron frequency, the motion conversion will always be incomplete, and the average magnetron radius will be larger to the average reduced cyclotron radius. Thus, although the central peak of the resonance will be almost unperturbed, the side peaks will be shifted in frequency in the same direction. This distortion is barely visible on the resonance itself, but its effect is much clearer on the fit residues shown in the bottom panel of Figure 4. The residues in all three cases (non-optimised and optimised first trap, optimised second trap) are close to 0 at the resonance frequency and the shift of the side peaks makes the residues antisymmetric.

When using the unoptimised set of potentials in the first trap, the distortion of the resonance induces a shift in the estimation of the cyclotron frequency of $2.4 * 10^{-7}$, while with optimised potentials, it drops to $2.0 * 10^{-8}$. Because

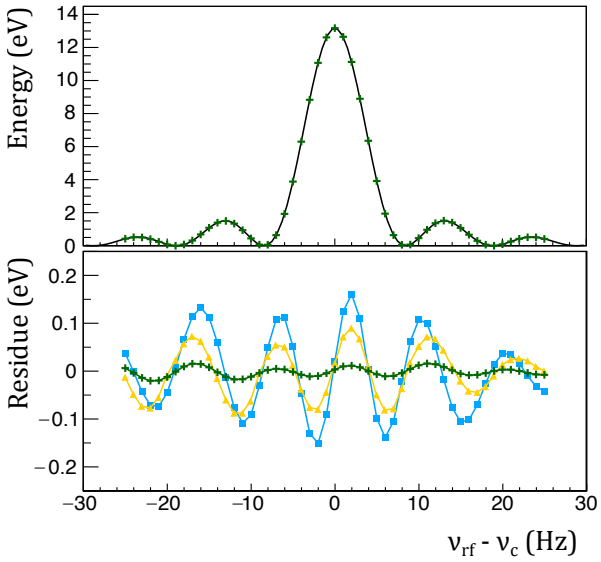

Figure 4: Top, kinetic energy of an ion after simulated quadrupolar excitation as a function of the detuning (first trap with optimised potentials). The shape of the resonance is remarkably well fitted by the theoretical curve $sin^2(\omega_B T_{rf})/\omega_B^2$ with $\omega_B = \frac{1}{2}\sqrt{(\omega_{rf}-\omega_c)^2 + k_0^2}$. : parameters used for the simulation are $z(0) = 2$ mm, $\rho_-(0) = 1.18$ mm, $A/Q = 250$, $V_{rf} = 25$ mV and $T_{rf} = 102.4$ ms. Bottom, fit residues of the resonances in a non-optimised first trap (blue squares), an optimised first trap (green crosses) and an optimised second trap (yellow triangles).

the trapped ions actually have a continuous distribution in z-amplitude and initial ρ_-, these shifts are responsible for resonance broadenings and systematic uncertainties of the same order. Thus the frequency shift in the first trap can be rightfully compared to the mass uncertainty of $2.9 * 10^{-8}$ and the accuracy of $3.6 * 10^{-8}$ obtained during the commissioning of the measurement tower [19].

The shift in the estimation of the cyclotron frequency in the cubic trap is $8.6 * 10^{-8}$. Once again, the larger error mostly results from the fact that the potential well in the detector-trap is much deeper than in the first trap. The residues and the systematic error would be lower if the ions had a smaller axial amplitude in the second trap. The inaccuracy difference could also be partially due to the difference in the $C_{4/6}$ factors, which is a consequence of the suboptimal aspect ratio of the second trap (*i.e.* the ratio of the width of the trap to its length) imposed by the size of the detectors.

In any case, it should be noticed that the reduced performances of the second trap are not caused by its cubic nature, since the average energy shift from the azimuthal components of the field over a turn of cyclotron/magnetron motion is 0, as is the resulting frequency shift. Thus the mass measurement capabilities of our detector trap seem mostly limited by the octupolar and dodecapolar components of the electric field and the depth of the potential well. This conclusion remains valid for any trap geometry featuring square-shaped electrodes. In our case the geometry of the silicon box and the potentials to be applied are constrained by the α-decay spectroscopy requirements.

5. Bunch Manipulation

In order to obtain more realistic expectations of the trap's performances, we simulated the flight path of a bunch of 100 ions through both the preparation and measurement traps. In the first trap the ions where exited by a dipolar pulse of 20 ms of amplitude 200 mV at the magnetron frequency, followed by a quadrupolar excitation of amplitude 45 mV for 250 ms at the cyclotron frequency. As the magnetron motion is slowly converted into reduced cyclotron motion, the latter is continuously dampened by helium buffer gas with a pressure of 10^{-4} mbar. The ion-gas interaction was simulated by a simple viscous damping model. The centering of the bunch is illustrated in Figure 5.

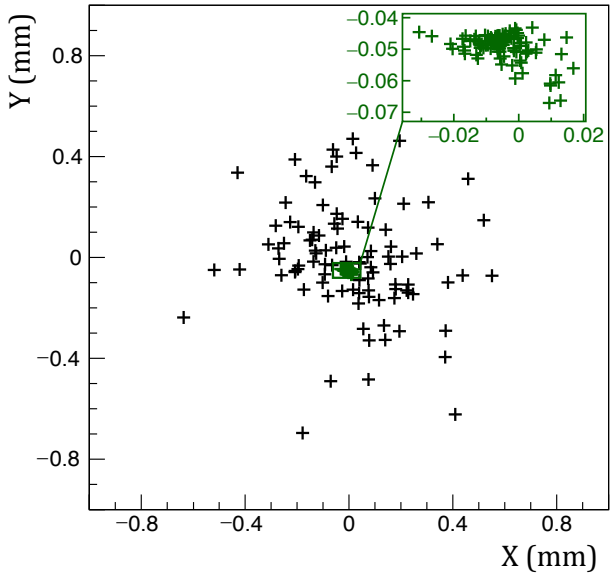

Figure 5: Bunch of 100 ions before (black) and after (green) cooling in the first trap.

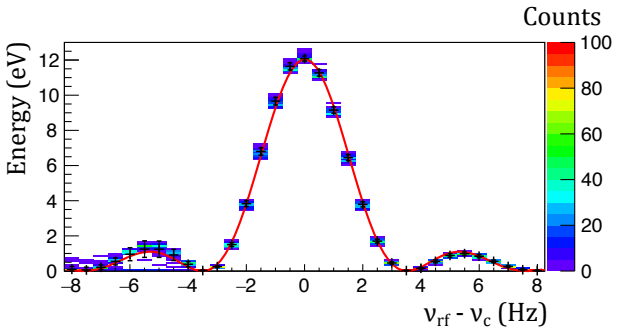

Figure 6: Energy distribution of the ion bunch as a function of the detuning frequency. The resonance is fitted with a reduced χ^2 of 1.3, owing to the trap imperfections.

The centered bunch was then transferred to the second trap and submitted to a ToF-ICR excitation pattern. A 10 ms dipolar magnetron excitation of 420 mV was followed by a 250 ms quadrupolar cyclotron excitation of 300 mV. The energy resonance for the complete ion bunch is shown in Figure 6. The measured frequency is shifted from the true cyclotron frequency by 10(10) mHz, i.e. a relative shift of $23(23) * 10^{-9}$ at mass $A = 250$, confirming the quality of the field. The results are better with a realistic bunch than with a single pure-motion ion as considered in the previous section. This can be explained by the fact that the simulated transfer of the ion bunch from the first trap to the second leaves the ions with an axial amplitude below 0.5 mm.

It is possible that the electric field imperfections in the real trap will turn out to be larger than what has been estimated, since our model does not account for misalignments or the possible charging of the small fraction of the PCB surface not covered by any electrode (see Fig. 1), though in the latter case, small plate-electrodes could be inserted to shield the insulating parts. However, our simulations show that this geometry itself is at least compatible with mass measurements with an uncertainty of a few 10^{-8}.

6. Conclusion and perspectives

In this paper we have described the goals and layout of a new double-trap assembly initially designed for in-trap decay spectroscopy and explored the possibility of using the same apparatus for precision mass measurements. The geometry and potentials of the novel trap have been adjusted to allow for dipolar and quadrupolar excitations required by the ToF-ICR and PI-ICR techniques. Simulations of the first trap with realistic bunches are consistent with the theory and simulations of the second trap support the feasibility of mass measurement with an uncertainty down to $23(23) * 10^{-9}$. Should the second trap of the novel tower be able to reach such precision, it could be used for mass measurements of exotic nuclei, wether they are α-emitters or not, and could provide valuable inputs in different regions of the chart of nuclides.

Mass measurements in the VHE and SHE regions allow to probe the evolution of shell structure and onset of deformation, and could be performed "simultaneously" with α-decay spectroscopy. Indeed, since an α-decaying ion is lost for mass measurement anyway, it does not matter wether its decay product is detected or not.

If the novel trap is limited to a precision of $\simeq 10^{-7}$ it could still measure masses of astrophysical interest, in particular those relevant to the paths of the rapid capture processes responsible for the abundances of elements heavier than iron. The first assembly will already measure masses of neutron-rich nuclei produced at ALTO, especially in the silver chain [20], and the second assembly could be tested for mass measurement as well. In DESIR, the S3-beams will provide many mass measurement opportunities along the rp-process line. Finally, mass measurements in the $10^{-7} - 10^{-8}$ precision range could be used as inputs or discrimination tests for the many nuclear interaction models that describe the exotic regions of the chart of nuclei to be covered by ALTO and S3.

7. Acknowledgements

This work was supported by CNRS and the P2IO LabEx (ANR-10-LABX-0038) in the framework "Investissements d'Avenir" (ANR-11-IDEX-0003-01) managed by the Agence Nationale de la Recherche (ANR, France).

8. References

[1] T. Eronen, A. Kankainen, J. Äystö, Ion traps in nuclear physics—recent results and achievements, Progress in Particle and Nuclear Physics 91 (2016) 259 – 293. doi:https://doi.org/10.1016/j.ppnp.2016.08.001.
URL http://www.sciencedirect.com/science/article/pii/S0146641016300436

[2] R. Orford, N. Vassh, J. A. Clark, G. C. McLaughlin, M. R. Mumpower, G. Savard, R. Surman, A. Aprahamian, F. Buchinger, M. T. Burkey, D. A. Gorelov, T. Y. Hirsh, J. W. Klimes, G. E. Morgan, A. Nystrom, K. S. Sharma, Precision mass measurements of neutron-rich neodymium and samarium isotopes and their role in understanding rare-earth peak formation, Phys. Rev. Lett. 120 (2018) 262702. doi:10.1103/PhysRevLett.120.262702.
URL https://link.aps.org/doi/10.1103/PhysRevLett.120.262702

[3] J. Karthein, K. Blaum, Precision mass measurements using the Phase-Imaging Ion-Cyclotron-Resonance detection technique, Master's thesis, University of Heidelberg, presented 2017 (2017).
URL https://cds.cern.ch/record/2300223

[4] K. Gulyuz, G. Bollen, M. Brodeur, R. A. Bryce, K. Cooper, M. Eibach, C. Izzo, E. Kwan, K. Manukyan, D. J. Morrissey, O. Naviliat-Cuncic, M. Redshaw, R. Ringle, R. Sandler, S. Schwarz, C. S. Sumithrarachchi, A. A. Valverde, A. C. C. Villari, High precision determination of the β decay Q_{ec} value of ^{11}C and implications on the tests of the standard model, Phys. Rev. Lett. 116 (2016) 012501. doi:10.1103/PhysRevLett.116.012501.
URL https://link.aps.org/doi/10.1103/PhysRevLett.116.012501

[5] J. Hakala, J. Dobaczewski, D. Gorelov, T. Eronen, A. Jokinen, A. Kankainen, V. S. Kolhinen, M. Kortelainen, I. D. Moore, H. Penttilä, S. Rinta-Antila, J. Rissanen, A. Saastamoinen, V. Sonnenschein, J. Äystö, Precision mass measurements beyond ^{132}Sn: Anomalous behavior of odd-even staggering of binding energies, Phys. Rev. Lett. 109 (2012) 032501. doi:10.1103/PhysRevLett.109.032501.
URL https://link.aps.org/doi/10.1103/PhysRevLett.109.032501

[6] G. Bollen, D. Davies, M. Facina, J. Huikari, E. Kwan, P. A. Lofy, D. J. Morrissey, A. Prinke, R. Ringle, J. Savory, P. Schury, S. Schwarz, C. Sumithrarachchi, T. Sun, L. Weissman, Experiments with thermalized rare isotope beams from projectile fragmentation: A precision mass measurement of the superallowed β emitter ^{38}Ca, Phys. Rev. Lett. 96 (2006) 152501. doi:10.1103/PhysRevLett.96.152501.
URL https://link.aps.org/doi/10.1103/PhysRevLett.96.152501

[7] R. Ringle, S. Schwarz, G. Bollen, Penning trap mass spectrometry of rare isotopes produced via projectile fragmentation at the lebit facility, International Journal of Mass Spectrometry 349-350 (2013) 87 – 93, 100 years of Mass Spectrometry. doi:https://doi.org/10.1016/j.ijms.2013.04.001.
URL http://www.sciencedirect.com/science/article/pii/S1387380613001279

[8] E. Minaya Ramirez, D. Ackermann, K. Blaum, M. Block, C. Droese, C. E. Düllmann, M. Eibach, S. Eliseev, E. Haettner, F. Herfurth, F. Heßberger, S. Hofmann, G. Marx, D. Nesterenko, Y. Novikov, W. Plaß, D. Rodríguez, C. Scheidenberger, L. Schweikhard, P. Thirolf, C. Weber, Recent developments for high-precision mass measurements of the heaviest elements at shiptrap, Nuclear Instruments and Methods in Physics Research Section B: Beam Interactions with Materials and Atoms 317 (2013) 501 – 505, xVIth International Conference on ElectroMagnetic Isotope Separators and Techniques Related to their Applications, December 2–7, 2012 at Matsue, Japan. doi:https://doi.org/10.1016/j.nimb.2013.07.055.
URL http://www.sciencedirect.com/science/article/pii/S0168583X13008732

[9] S. Kreim, D. Atanasov, D. Beck, K. Blaum, C. Böhm, C. Borgmann, M. Breitenfeldt, T. Cocolios, D. Fink, S. George, A. Herlert, A. Kellerbauer, U. Köster, M. Kowalska, D. Lunney, V. Manea, E. M. Ramirez, S. Naimi, D. Neidherr, T. Nicol, R. Rossel, M. Rosenbusch, L. Schweikhard, J. Stanja, F. Wienholtz, R. Wolf, K. Zuber, Recent exploits of the isoltrap mass spectrometer, Nuclear Instruments and Methods in Physics Research Section B: Beam Interactions with Materials and Atoms 317 (2013) 492 – 500, xVIth International Conference on ElectroMagnetic Isotope Separators and Techniques Related to their Applications, December 2–7, 2012 at Matsue, Japan. doi:https://doi.org/10.1016/j.nimb.2013.07.072.
URL http://www.sciencedirect.com/science/article/pii/S0168583X13009014

[10] J. Van Schelt, D. Lascar, G. Savard, J. A. Clark, P. F. Bertone, S. Caldwell, A. Chaudhuri, A. F. Levand, G. Li, G. E. Morgan, R. Orford, R. E. Segel, K. S. Sharma, M. G. Sternberg, First results from the caribu facility: Mass measurements on the *r*-process path, Phys. Rev. Lett. 111 (2013) 061102. doi:10.1103/PhysRevLett.111.061102.
URL https://link.aps.org/doi/10.1103/PhysRevLett.111.061102

[11] V. Kolhinen, T. Eronen, D. Gorelov, J. Hakala, A. Jokinen, K. Jokiranta, A. Kankainen, M. Koikkalainen, J. Koponen, H. Kulmala, M. Lantz, A. Mattera, I. Moore, H. Penttilä, T. Pikkarainen, I. Pohjlainen, M. Reponen, S. Rinta-Antila, J. Rissanen, C. R. Triguero, K. Rytkönen, A. Saastamoinen, A. Solders, V. Sonnenschein, J. Äystö, Recommissioning of jyfltrap at the new igisol-4 facility, Nuclear Instruments and Methods in Physics Research Section B: Beam Interactions with Materials and Atoms 317 (2013) 506 – 509, xVIth International Conference on ElectroMagnetic Isotope Separators and Techniques Related to their Applications, December 2–7, 2012 at Matsue, Japan. doi:https://doi.org/10.1016/j.nimb.2013.07.050.
URL http://www.sciencedirect.com/science/article/pii/S0168583X13008641

[12] A. Chaudhuri, C. Andreoiu, M. Brodeur, T. Brunner, U. Chowdhury, S. Ettenauer, A. T. Gallant, A. Grossheim, G. Gwinner, R. Klawitter, A. A. Kwiatkowski, K. G. Leach, A. Lennarz, D. Lunney, T. D. Macdonald, R. Ringle, B. E. Schultz, V. V. Simon, M. C. Simon, J. Dilling, Titan: an ion trap for accurate mass measurements of ms-half-life nuclides, Applied Physics B 114 (1) (2014) 99–105. doi:10.1007/s00340-013-5618-8.
URL https://doi.org/10.1007/s00340-013-5618-8

[13] J. Ketelaer, G. Audi, T. Beyer, K. Blaum, M. Block, R. B. Cakirli, R. F. Casten, C. Droese, M. Dworschak, K. Eberhardt, M. Eibach, F. Herfurth, E. Minaya Ramirez, S. Nagy, D. Neidherr, W. Nörtershäuser, C. Smorra, M. Wang, Mass measurements on stable nuclides in the rare-earth region with the penning-trap mass spectrometer triga-trap, Phys. Rev. C 84 (2011) 014311. doi:10.1103/PhysRevC.84.014311.
URL https://link.aps.org/doi/10.1103/PhysRevC.84.014311

[14] E. Minaya Ramirez, P. Alfaurt, M. Aouadi, P. Ascher, B. Blank, K. Blaum, J.-F. Cam, P. Chauveau, L. Daudin, P. Delahaye, F. Delalee, P. Dupré, S. E. Abbeir, M. Gerbaux, S. Grévy, H. Guérin, D. Lunney, F. Metz, S. Naimi, L. Perrot, A. de Roubin, L. Serani, B. Thomas, J.-C. Thomas, Conception of piperade: A high-capacity penning-trap mass separator for high isobaric contamination at desir, Nuclear Instruments and Methods in Physics Research Section B: Beam Interactions with Materials and Atoms 376 (2016) 298 – 301, proceedings of the XVIIth International Conference on Electromagnetic Isotope Separators and Related Topics (EMIS2015), Grand Rapids, MI, U.S.A., 11-15 May 2015. doi:https://doi.org/10.1016/j.nimb.2016.01.044.
URL http://www.sciencedirect.com/science/article/pii/S0168583X16001051

[15] M. Mehlman, P. D. Shidling, R. Burch, E. Bennett, B. Fenker, D. Melconian, Status of the tamutrap facility and initial characterization of the rfq cooler/buncher, Hyperfine Interactions 235 (1) (2015) 77–86. doi:10.1007/s10751-015-1187-z.
URL https://doi.org/10.1007/s10751-015-1187-z

[16] R. X. Schüssler, M. Door, A. Rischka, H. Bekker, J. R. C. López-Urrutia, P. Filianin, S. Eliseev, Y. N. Novikov, S. Sturm, S. Ulmer, K. Blaum, Recent developments at the high-precision mass spectrometer pentatrap, JPS Conference Proceedings 18 (011020). arXiv:https://journals.jps.jp/doi/pdf/10.7566/JPSCP.18.011020, doi:10.7566/JPSCP.18.011020.
URL https://journals.jps.jp/doi/abs/10.7566/JPSCP.18.011020

[17] W. Huang, Y. Tian, J. Wang, Y. Sun, Y. Wang, Y. Wang, J. Zhao, W. Wu, L. Ma, Y. He, H. Xu, G. Xiao, Status of lanzhou penning trap for accurate mass measurements, Nuclear Instruments and Methods in Physics Research Section B: Beam Interactions with Materials and Atoms 317 (2013) 528 – 531, xVIth International Conference on ElectroMagnetic Isotope Separators and Techniques Related to their Applications, December 2–7, 2012 at Matsue, Japan. doi:https://doi.org/10.1016/j.nimb.2013.07.041.
URL http://www.sciencedirect.com/science/article/pii/S0168583X13008549

[18] D. Lunney, New mass measurements with trapped (radioactive) ions and related fundamental physics, Hyperfine Interactions 240 (1) (2019) 48. doi:10.1007/s10751-019-1581-z.
URL https://doi.org/10.1007/s10751-019-1581-z

[19] V. Kolhinen, M. Bussmann, E. Gartzke, D. Habs, J. Neumayr, C. Schürmann, J. Szerypo, P. Thirolf, Commissioning of the double penning trap system mlltrap, Nuclear Instruments and Methods in Physics Research Section A: Accelerators, Spectrometers, Detectors and Associated Equipment 600 (2) (2009) 391 – 397. doi:https://doi.org/10.1016/j.nima.2008.12.004.
URL http://www.sciencedirect.com/science/article/pii/S0168900208018081

[20] E. M. Ramirez, P. Chauveau, S. Franchoo, J. Ljungvall, A. Lopez-Martens, D. Lunney, M. MacCormick, L. Perrot, P. Thirolf, New program for measuring masses of silver isotopes near the n=82 shell closure with mlltrap at alto, Nuclear Instruments and Methods in Physics Research Section B: Beam Interactions with Materials and Atomsdoi:https://doi.org/10.1016/j.nimb.2019.04.075.
URL http://www.sciencedirect.com/science/article/pii/S0168583X19302599

[21] P. Chauveau, S. Franchoo, K. Hauschild, J. Ljungvall, A. Lopez-Martens, D. Lunney, M. MacCormick, E. M. Ramirez], P. Thirolf, C. Weber,

Application of in-trap spectroscopy to lifetime measurements with mlltrap, Nuclear Instruments and Methods in Physics Research Section B: Beam Interactions with Materials and Atoms 463 (2020) 371 – 374. doi:https://doi.org/10.1016/j.nimb.2019.04.057.
URL http://www.sciencedirect.com/science/article/pii/S0168583X19302423

[22] C. Weber, R. Meißner, P. Müller, P. Thirolf, Recent developments at mlltrap: Improving the system for mass measurements and in-trap observation of nuclear decays, Nuclear Instruments and Methods in Physics Research Section B: Beam Interactions with Materials and Atoms 317 (2013) 532 – 536, xVIth International Conference on ElectroMagnetic Isotope Separators and Techniques Related to their Applications, December 2–7, 2012 at Matsue, Japan. doi:https://doi.org/10.1016/j.nimb.2013.07.048.
URL http://www.sciencedirect.com/science/article/pii/S0168583X13008616

[23] C. Weber, P. Müller, P. Thirolf, Developments in penning trap (mass) spectrometry at mlltrap: Towards in-trap decay spectroscopy, International Journal of Mass Spectrometry 349-350 (2013) 270 – 276, 100 years of Mass Spectrometry. doi:https://doi.org/10.1016/j.ijms.2013.05.006.
URL http://www.sciencedirect.com/science/article/pii/S1387380613001759

[24] C. Weber, R. Meißner, P. Müller, P. G. Thirolf, Status of the mlltrap setup and future plans, Hyperfine Interactions 227 (1) (2014) 247–258. doi:10.1007/s10751-014-1044-5.
URL https://doi.org/10.1007/s10751-014-1044-5

[25] B. Blank, S. Grévy, P. Thirolf, C. Weber, Perspectives for mass spectrometry at the desir facility of spiral2, International Journal of Mass Spectrometry 349-350 (2013) 264 – 269, 100 years of Mass Spectrometry. doi:https://doi.org/10.1016/j.ijms.2013.03.006.
URL http://www.sciencedirect.com/science/article/pii/S1387380613000821

[26] [online][link].

[27] F. Déchery, H. Savajols, M. Authier, A. Drouart, J. Nolen, D. Ackermann, A. Amthor, B. Bastin, A. Berryhill, D. Boutin, L. Caceres, M. Coffey, O. Delferrière, O. Dorvaux, B. Gall, K. Hauschild, A. Hue, B. Jacquot, N. Karkour, B. Laune, F. L. Blanc, N. Lecesne, A. Lopez-Martens, F. Lutton, S. Manikonda, R. Meinke, G. Olivier, J. Payet, J. Piot, O. Pochon, V. Prince, M. Souli, G. Stelzer, C. Stodel, M.-H. Stodel, B. Sulignano, E. Traykov, D. Uriot, The super separator spectrometer s3 and the associated detection systems: Sirius & leb-reglis3, Nuclear Instruments and Methods in Physics Research Section B: Beam Interactions with Materials and Atoms 376 (2016) 125 – 130, proceedings of the XVIIth International Conference on Electromagnetic Isotope Separators and Related Topics (EMIS2015), Grand Rapids, MI, U.S.A., 11-15 May 2015. doi:https://doi.org/10.1016/j.nimb.2016.02.036.
URL http://www.sciencedirect.com/science/article/pii/S0168583X1600166X

[28] M. König, G. Bollen, H.-J. Kluge, T. Otto, J. Szerypo, Quadrupole excitation of stored ion motion at the true cyclotron frequency, International Journal of Mass Spectrometry and Ion Processes 142 (1) (1995) 95 – 116. doi:https://doi.org/10.1016/0168-1176(95)04146-C.
URL http://www.sciencedirect.com/science/article/pii/016811769504146C

[29] S. Eliseev, K. Blaum, M. Block, A. Dörr, C. Droese, T. Eronen, M. Goncharov, M. Höcker, J. Ketter, E. M. Ramirez, D. A. Nesterenko, Y. N. Novikov, L. Schweikhard, A phase-imaging technique for cyclotron-frequency measurements, Applied Physics B 114 (1) (2014) 107–128. doi:10.1007/s00340-013-5621-0.
URL https://doi.org/10.1007/s00340-013-5621-0

[30] H. Wollnik, M. Przewloka, Time-of-flight mass spectrometers with multiply reflected ion trajectories, International Journal of Mass Spectrometry and Ion Processes 96 (3) (1990) 267 – 274. doi:https://doi.org/10.1016/0168-1176(90)85127-N.
URL http://www.sciencedirect.com/science/article/pii/016811769085127N

[31] A. Makarov, Electrostatic axially harmonic orbital trapping: a high-performance technique of mass analysis, Analytical Chemistry 72 (6) (2000) 1156–1162, pMID: 10740853. arXiv:https://doi.org/10.1021/ac991131p, doi:10.1021/ac991131p.
URL https://doi.org/10.1021/ac991131p

[32] W. Paul, Electromagnetic traps for charged and neutral particles, Rev. Mod. Phys. 62 (1990) 531–540. doi:10.1103/RevModPhys.62.531.
URL https://link.aps.org/doi/10.1103/RevModPhys.62.531

[33] L. S. Brown, G. Gabrielse, Geonium theory: Physics of a single electron or ion in a penning trap, Rev. Mod. Phys. 58 (1986) 233–311. doi:10.1103/RevModPhys.58.233.
URL https://link.aps.org/doi/10.1103/RevModPhys.58.233

[34] G. Bollen, R. B. Moore, G. Savard, H. Stolzenberg, The accuracy of heavyion mass measurements using time of flightion cyclotron resonance in a penning trap, Journal of Applied Physics 68 (9) (1990) 4355–4374. arXiv:https://doi.org/10.1063/1.346185, doi:10.1063/1.346185.
URL https://doi.org/10.1063/1.346185

[35] J. Ketter, T. Eronen, M. Höcker, S. Streubel, K. Blaum, First-order perturbative calculation of the frequency-shifts caused by static cylindrically-symmetric electric and magnetic imperfections of a penning trap, International Journal of Mass Spectrometry 358 (2014) 1 – 16. doi:https://doi.org/10.1016/j.ijms.2013.10.005.
URL http://www.sciencedirect.com/science/article/pii/S1387380613003722

[36] K. Blaum, High-accuracy mass spectrometry with stored ions, Physics Reports 425 (1) (2006) 1 – 78. doi:https://doi.org/10.1016/j.physrep.2005.10.011.
URL http://www.sciencedirect.com/science/article/pii/S0370157305004643

[37] E. Minaya Ramirez, An investigation of the accuracy of the pi-icr technique at shiptrap by a measurement of the mass difference between ¡sup¿132¡/sup¿xe and ¡sup¿131¡/sup¿xe, JPS Conference Proceedings 6 (020023). arXiv:https://journals.jps.jp/doi/pdf/10.7566/JPSCP.6.020023, doi:10.7566/JPSCP.6.020023.
URL https://journals.jps.jp/doi/abs/10.7566/JPSCP.6.020023

[38] D. A. Nesterenko, T. Eronen, A. Kankainen, L. Canete, A. Jokinen, I. D. Moore, H. Penttilä, S. Rinta-Antila, A. de Roubin, M. Vilen, Phase-imaging ion-cyclotron-resonance technique at the jyfltrap double penning trap mass spectrometer, The European Physical Journal A 54 (9) (2018) 154. doi:10.1140/epja/i2018-12589-y.
URL https://doi.org/10.1140/epja/i2018-12589-y

[39] Simion charged particle optics simulation software. [online].

[40] F. James, M. Roos, Minuit - a system for function minimization and analysis of the parameter errors and correlations, Computer Physics

Communications 10 (6) (1975) 343 – 367. doi:https://doi.org/10.1016/0010-4655(75)90039-9.
URL http://www.sciencedirect.com/science/article/pii/0010465575900399

[41] S. Eliseev, K. Blaum, M. Block, C. Droese, M. Goncharov, E. Minaya Ramirez, D. A. Nesterenko, Y. N. Novikov, L. Schweikhard, Phase-imaging ion-cyclotron-resonance measurements for short-lived nuclides, Phys. Rev. Lett. 110 (2013) 082501. doi:10.1103/PhysRevLett.110.082501.
URL https://link.aps.org/doi/10.1103/PhysRevLett.110.082501